**Details**

Title: Coulomb Threshold Rate-and-State Model for Fault Reactivation: Application to induced seismicity at Groningen

Authors

Heimisson, Elias; Caltech/ETH Zurich, Swiss Seismological Service
Smith, Jonathan; California Institute of Technology, Seismological Laboratory
Avouac, Jean-Phillipe; California Institute of Technology, Geology and Planetary Science
Bourne, Stephen; Shell Global Solutions International,

Contact: elias.heimisson@sed.ethz.ch

submitted to *Geophys. J. Int.*

# Coulomb Threshold Rate-and-State Model for Fault Reactivation: Application to induced seismicity at Groningen

Elías R. Heimisson[1,2⋆], Jonathan D. Smith[1], Jean-Philippe Avouac[1], Stephen J. Bourne[3]

[1] *Division of Geological and Planetary Sciences, California Institute of Technology, Pasadena, 91106, California, USA.*

[2] *Now at: Swiss Seismological Service, ETH Zurich, Zurich, Switzerland*

[3] *Shell Global Solutions, Amsterdam, Netherlands*

**SUMMARY**

A number of recent modeling studies of induced seismicity have used the rate-and-state friction model of Dieterich (1994) to account for the fact that earthquake nucleation is not instantaneous. Notably, the model assumes a population of seismic sources accelerating towards instability with a distribution of intial slip speeds such that they would produce earthquakes steadily in absence of any perturbation to the system. This assumption may not be valid in typical intra-plate settings where most examples of induced seismicity occur, since these regions have low stressing rates and initially low seismic activity. The goal of this paper is twofold. First, to derive a revised Coulomb rate-and-state model, which takes into account that seismic sources can be initially far from instability. Second, to apply and test this new model, called the Threshold rate-and-state model, on the induced seismicity of the Groningen gas field in the Netherlands. Stress changes are calculated based on a model of reservoir compaction (Smith et al. 2019) since the onset of gas production. We next compare the seismicity predicted by our threshold model and Dieterich (1994)'s model with the observations. The two models yields comparable spatial distributions of earthquakes in good agreement with the observations. We find however that the Threshold model provides a better fit to the observed time-varying seismicity rate than Dieterich (1994)'s model, and reproduces better the onset, peak, and decline of the observed seismicity rate. We compute the maximum magnitude expected for each model given the Gutenberg-Richter distribution and compare to the observations. We find that the Threshold model both shows better agreement with the observed maximum magnitude and provides results consistent with lack of observed seismicity prior to 1993. We carry out analysis of the model fit using a Chi-squared reduced statistics and find that the model fit is dramatically improved by smoothing the seismicity rate. We interpret this finding as possibly suggesting an influence of source interactions, or clustering, on a long time-scale of about 3–5 year.

**Key words:** Earthquakes; Microseismicity; Seismic-event rates; Earthquake-source mechanism; b values; Stress distribution

## 1 INTRODUCTION

Many prominent examples of anthropogenically induced seismicity occur away from tectonically active regions in intraplate settings where strain rates and background seismic activity is low. Two well-known examples are the waste-water injection-induced seismicity in Oklahoma (Ellsworth 2013) and the extraction induced seismicity in the Groningen gas field in the Netherlands with, remarkably, no detected historical seismicity (Dost et al. 2017). These two examples, have in common that the onset of induced seismicity occurred at a significant time-lag after the start of injection or production and stress changes in the crust became significant. In Oklahoma the onset of an anomalous seismicity rate occurred about 13 years after injection started (Zhai et al. 2019), but gas was extracted for about 25 years from the Groningen gas field before any detected earthquake occurred (Bourne et al. 2014; Smith et al. 2019) (Figure 1a).

In order to understand the interplay of injection or extraction and the observed induced seismicity, a number of recent studies have coupled mechanical models of crustal stress changes and the seismicity rate theory of Dieterich (1994) (e.g., Zhai et al. 2019; Candela et al. 2019; Norbeck & Rubinstein 2018; Richter et al. 2020). The theory of Dieterich (1994) is based on empirically derived rate-and-state friction law (e.g. Dieterich 1979; Ruina 1983; Marone 1998). However, in the process of obtaining

⋆ Corresponding author: eheimiss@caltech.edu

an attractive expression and maintaining mathematical tractability, several assumptions are made by Dieterich (1994) and further investigated by Heimisson & Segall (2018). A critical assumption is sometimes referred to as “the no-healing limit”, or the “well above steady-state limit”. Dieterich (1994) indeed assumes that some seismic sources in the system must be well above steady-state, meaning that they are accelerating towards instability, regardless of any perturbations to the system. He further assumes that the distribution of their initial state is such that they would result in a steady seismicity rate for a constant background stressing rate. If all the seismic sources are ’healing’ with time, meaning strengthening due to the evolution of the state variable, then the theory is not strictly valid. We refer the reader to Appendix A of a mathematical definition of the well above steady state limit. Heimisson & Segall (2018) demonstrated a mitigating effect whereby sources initially below steady state can participate in an aftershock sequence (as if they where initially above steady-state) if the step change in stress caused by the main-shock brings the sources above steady state. However, for a more gradual stress changes this effect may not be invoked to justify the well above steady-state limit.

Regions, such as Oklahoma and Groningen, located in a intra-plate setting with low stressing rates, where induced seismicity only manifests over a decade after start of injection or extraction appear to be in direct contradiction to the well above steady-state limit. As a result, Zhai et al. (2019) found that in order to fit they seismicity rate in Oklahoma they introduced a, somewhat ad hoc, “critical time”, before which stress perturbations to the system are ignored. Candela et al. (2019) used the Dieterich (1994) model for Groningen and obtained an acceptable fit with observed seismicity rate. They, however, had to the set initial conditions such that the seismicity rate reached a constant steady-state value only in 1993. While they acknowledge that this is probably and oversimplification, it demonstrates again that the Dieterich (1994) model requires ad hoc modifications in order to be compatible in this kind of a intra-plate setting. Such modifications are typically not needed in more active settings.

Bourne et al. (2018) proposed that the lag in seismicity at Groningen could be explained a probabilistic Coulomb failure stress distribution and thus initially the system is generally far from failure, but as continued stressing occurs from extraction more sources are brought to failure. The perspective of Bourne et al. (2018), and continued work by Smith et al. (2021), contrasts that of Candela et al. (2019) by postulating a failure stress distribution and thus a threshold stress for activation, whereas Candela et al. (2019) used the rate-and-state theory of Dieterich (1994) and thus had no threshold stress. These two perspective imply different possible explanation of the lag in seismicity. First, that a stress threshold is needed to initiate failure, the second that a lag in initiation of seismicity is caused by the time-dependence of friction and that the lag could reflect the nucleation time.

In this paper we resolve this problem by demonstrating the threshold effect introduced when a population of seismic sources obeying rate-and-state friction and initially far from instablity is con-

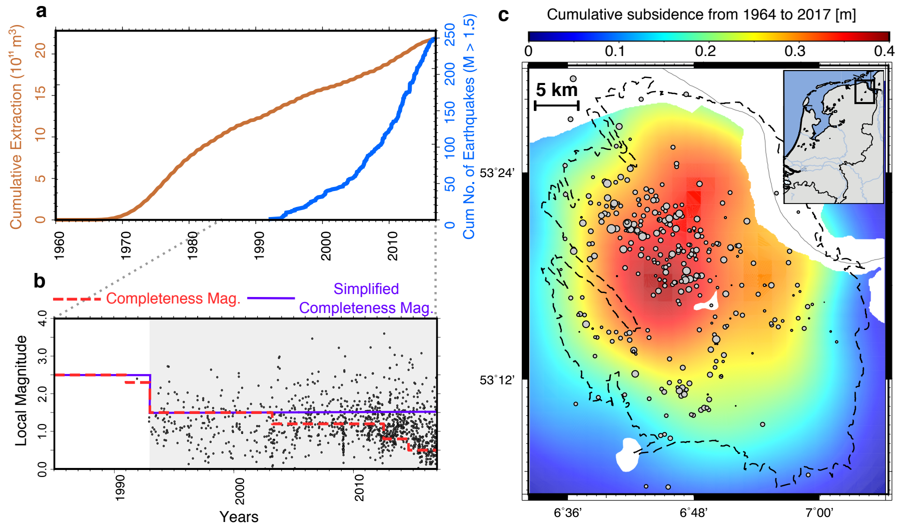


**Figure 1.** Groningen gas field data overview. a: Cumulative extraction and cumulative number of events with time. Note the large lag between first detected earthquake and the start of production. b: Earthquakes with time along with estimated completeness threshold. In the study we use the more conservative and simplified thresholds, indicated in purple, to filter the catalog. Only seismic observations in the shaded time-period are used to constrain models. We make no assumption about seismicity before 1993. c: Subsidence map used to constrain Coulomb stress model (see Smith et al. 2019; Bourne & Oates 2017)

.

sidered. We apply this threshold rate-and-state model to the Groningen dataset and demonstrate that the model outperforms Dieterich (1994)'s model applied without ad hoc modifications. The paper has three main parts, first we discuss the main features of proposed model and some implications. The model derivation itself is presented in Appendix A and B. Second, we apply the model to the Groningen dataset and compare to the original Dieterich (1994) theory by modeling annual seismicity rates. Finally, we offer a discussion of the broader implications of our findings.

## 2 THEORY

Here we present the new model, contrast it to the original theory by Dieterich (1994) and discuss some implications. The mathematical derivation is detailed in appendix A and B.

In Appendix A we derive an expression for the time to activation of a seismic source, represented by a spring-slider, which is initially well below steady state or healing with time. This initial condition differs from that of Dieterich (1994) who assumes that each source is initially well above steady state, and thus weakening and accelerating towards instability. We find that the time that the source is elevated above steady state and begins weakening and accelerating, which is the state assumed to be the initial state by Dieterich (1994), is a simple stress threshold criterion.

In Appendix B, we use the approach of Heimisson & Segall (2018) to derive the seismicity rate for a population of seismic sources that start out initially below steady state and move above steady state with time.

Thus in Appendix B we arrive at the following equation:

$$
\begin{aligned}
\frac{R}{r} &= \frac{\exp\left(\frac{\Delta S(t)-\Delta S_c}{A\sigma_0}\right)}{\frac{1}{t_a}\int_{t_b}^{t}\exp\left(\frac{\Delta S(t')-\Delta S_c}{A\sigma_0}\right)dt'+1} && \text{if } t \geq t_b \\
\frac{R}{r} &= 0 && \text{if } t < t_b
\end{aligned}
\qquad (1)
$$

where $R$ is the seismicity rate of a population of 'dormant' or 'inactive' seismic sources at times $t < t_b$. $\Delta S(t) = \Delta\tau(t) + \mu\Delta\sigma(t)$ is a modified Coulomb stress where the effective coefficient of friction is $\mu = \tau_0/\sigma_0 - \alpha$ where $\tau_0$ and $\sigma_0$ are the initial shear and normal stresses respectively acting on the population at $t = 0$ and $\alpha$ is the the Linker & Dieterich (1992) constant. $\Delta S_c$ is the threshold Coulomb stress. In Appendix A we show that a seismic source at well-below steady-state will is moved above steady state at a threshold Coulomb stress that is independent of the stressing history prior to reaching the threshold. The time $t_b$ at which the threshold stress is reached, is then given by $\Delta S(t = t_b) = \Delta S_c$. We thus stress that $t_b$ is fully determined by $\Delta S_c$ and not an independent parameter. A major difference with the 'critical time' of Zhai et al. (2019) is that if the stressing rate is non uniform then $t_b$ represents a lag that should vary in space. Finally, as in Dieterich (1994), $A\sigma_0$ is a characteristic stress where $A$ is a constitutive parameter related to the direct effect. $t_a = A\sigma_0/\dot{s}_b$, where $\dot{s}_b$ is the background Coulomb stressing rate, is the characteristic time of aftershock decay following a step increase of stress. Background seismicity rate $r$ is defined as the seismicity rate that the population would reach if continuously stresses at $\dot{s}_b$ until $\Delta S_c$ is reached. Thus unlike the Dieterich (1994) theory the background rate $r$ is not observable prior to reaching $\Delta S_c$. By definition, if $t < t_b$ and thus the $\Delta S(t) < \Delta S_c$, then $R = 0$ since no seismic sources have been moved above steady state.

Following Heimisson & Segall (2018) it is easy to show that the corresponding Dieterich (1994) version of equation 1 is

$$
\frac{R}{r} = \frac{\exp\left(\frac{\Delta S(t)}{A\sigma_0}\right)}{\frac{1}{t_a}\int_{0}^{t}\exp\left(\frac{\Delta S(t')}{A\sigma_0}\right)dt'+1}. \qquad (2)
$$

Comparison of equations 1 and 2 reveals that if $\Delta S_c = 0$ and thus $t_b = 0$ the two equations are the same. Dieterich (1994)'s model is thus a special case of equation 1 in the limit that of no stress threshold.

In order to gain some further insight into equation 1 we derive Omori's law of aftershocks in absence of postseismic reloading. In other words, we explore a special case of a instantaneous jump $\Delta S$ in stress at t=0. If the $\Delta S > \Delta S_c$ then $t_b = 0$. Then equation 1 gives:

$$\frac{R}{r} = \frac{1}{t/t_a + e^{(\Delta S_c - \Delta S)/A\sigma_0}}, \tag{3}$$

which we contrast to the empirical Omori-Utsu law $R = a/(t+c)$, where the decay rate is taken as 1/t. As was previously discussed, the corresponding Dieterich (1994) equation is obtain by simply setting $\Delta S_c = 0$. We thus see that the $c$ parameter in Omori's law depends on $\Delta S_c$. This results in a lower initial rate of earthquakes in the aftershocks sequence and longer time until the onset of the characteristic 1/t decays than compared to Dieterich (1994) equation.

We recognize that if $\Delta S = \Delta S_c$, then $R = r$ and thus no aftershock sequence occurs. This is consistent with the simulations and analysis of Heimisson & Segall (2018), which show that only seismic source already above or elevated above steady state participate in the aftershock sequence.

## 3 APPLICATION TO GRONINGEN

In this section we compare the threshold rate-and-state model (equation 1) to the original Dieterich (1994) model (equation 2)

### 3.1 Groningen: Background

Gas production at the Groningen gas field, in the northeast of the Netherlands (Figure 1c, inset) began in 1963 with the most rapid gas extraction in the 70's and a fairly steady extraction rate since 1980 (Figure 1a). In spite of over two decades of extraction and substantial field compaction (Bourne & Oates 2017; Smith et al. 2019), the first detected earthquake occurred in the 90's (Figure 1a, b). At the time the seismic network has a magnitude of completeness around 2.3 Dost et al. (2017)(see. Figure 1b) , and thus some seismicity may have gone undetected, but in 1993 the seismic network improved greatly and the completeness magnitude was reduced to 1.5. In the following years, improvements to the seismic network have further lowered the completeness magnitude. In the following modeling and analysis, we make the conservative assumption that the completeness magnitude prior to 1993 was 2.5 and 1.5 after 1993 (Figure 1b, purple line).

The gas production has caused a substantial compaction of the gas field, which has resulted in subsidence of nearly $0.4$ m at its maximum (Figure 1c), and observable seismicity depths ranging from the reservoir caprock (Smith et al. 2020) to within the reservoir (Willacy et al. 2019; Dost et al. 2017). Smith et al. (2019) have integrated several different geodetic measurement techniques, used through time to monitor the compaction of the reservoir. Using a pressure depletion simulations from Nederlandse Aardolie Maatschappij (2013), they determined the uniaxial compressibility of the reservoir and found it to be variable in space but pressure-independent (constant in time). Smith et al. (2021) used the pressure variations and spatially variable compaction of the reservoir to calculate spatial and temporal variations of Coulomb stress. We use the coulomb stress changes from this study to compute $\Delta S(t)$ in equations (1) and (2). We stress that $\Delta S(t)$ is a function of easting and northing, which we will denote by $x$ and $y$ respectively. However, all parameters for the purpose of fitting, as is discussed in the following section, are treated as spatially and temporally constant.

### 3.2 Methods

For model comparison we follow strategy of Smith et al. (2021), which is briefly outlined here. Earthquakes are placed in yearly bins (Figure 2, red line) following a magnitude filtering for completeness of 1.5.

We quantify misfit using a Gaussian log-likelihood function

$$\log(p(\boldsymbol{m}|\boldsymbol{R}^o)) = -\frac{1}{2}\sum_{i=1993}^{i=2016}\left(R_i^o - \int_{\Sigma} R(\boldsymbol{m}, i, x, y)dxdy\right)^2, \tag{4}$$

where $R(\boldsymbol{m}, i)$ is the model predicted rate density in year $i$ (equation 1 or 2), where $\boldsymbol{m}$ is the vector of model parameters. $R_i^o$ is the observed rate in year $i$. Integration in easting, $x$, and northing $y$, is carried over the area $\Sigma$, which is shown by the outlines of the gasfield in Figure 1c. In practice, the integration is done by splitting the area up in square blocks of 0.25 km$^2$. Then take center Coulomb stress in each block as constant over the area, use the time-history of the Coulomb stress at the location and compute rate density from equation 1 or 2 assuming that $r$ represents background rate per unit area. Finally we sum all the blocks. In equation 4 we have assumed that the standard deviation of the observed seismicity rate is 1 event/year, which is why weighing each term by a variance is omitted in equation 4. Further, the prior probability of the model parameters is uniform and thus only scales the likelihood function by a constant factor as long as the priors are satisfied. The choice of data standard deviation of 1 is justified only when the rate is estimated by sampling a Poissonian distribution. Then $R_i^o$ represents the sample mean of the observed rate in each time bin. Because we estimate the seismicity rate by binning the statistics of the observed rate is not governed by the Poissonian distribution but by the corresponding sampling distribution of the mean. The expectation value of the sampling distribution is simply $\lambda$ where is the $\lambda$ is the expectation value of the Poisson distribution and thus $\lambda \approx N$, where N is the number of events in a fixed time-interval. However the variance of the sample mean is $\lambda/N$ and thus the variance is $\approx 1$ (see Appendix C for details). Further, we assume sufficiently many events have occurred in each bin to invoke the central limit theorem such that we can use a Gaussian log-likelihood function (see also Smith et al. 2021). We stress that the choice of variance model should be considered as minimum variance model and the resulting constrains on model parameters as of the narrowest confidence intervals that can be reasonably obtained. We discuss and provide further justification of this choice in Section 4.2

We us an ensemble Markov Chain Monte Carlo (MCMC) algorithm (Goodman & Weare 2010; Foreman-Mackey et al. 2013) to sample the probability distribution in equation (4) under the constrains of uniform model parameter priors. The uniform priors are placed as follows. $r$ between $10^{-6.2}$ to $10^{-2.6}$ events/(year km$^2$). The upper limit is selected as such under that the seismicity in 1993 would correspond to background activity. The lower limit is selected assuming that the field would produce 1 event per 1000 years under background conditions. $A\sigma_0$ is selected between 0.001 to 1 MPa, the range is selected to reflect the typical range from aftershock studies 0.01 to 0.1 MPa (Hainzl et al. 2010), but with considerable additional uncertainty since such values are constrained in very different tectonic settings from the Groningen gas field. $t_a$ has been set between 0.5 years to 10000 years. In aftershock studies this parameter ranges from less than a year to tens of years (Dieterich 1994; Cattania et al. 2014). However, much larger values have been used in induced seismicity modeling. For example Zhai et al. (2019) used $t_a = 6600$ year as their reference model for Oklahoma. We thus choose a prior to reflect this large range of values used elsewhere. However, we acknowledge that our yearly average treatments of seismicity rates would likely prevent us from resolving small values of $t_a$ and the finite time of the observation period should also prevent resolving very large values of $t_a$. See further discussion in the next section.

### 3.3 Results

Comparison of the MCMC sampling are shown in Figure 2 where results using equation 1 and 2 that is the new Threshold model and the original Dieterich (1994) model. We have highlighted the *maximum a posteriori* or MAP model in blue, which here maximizes the likelihood function and satisfies the priors. Comparison of the data and the MAP reveals that the threshold model shows considerably better agreement from 1993 – 2003, where the Dieterich (1994) model overpredicts the rate systematically. Further from 2014-2017 a decline in the rate is observed in the data and the threshold model prediction, but not in the Dieterich (1994) model. The model of Candela et al. (2019) similarly fails to match the observed decline. Another striking difference occurs prior to 1993 and thus before the time range used to constrain the model. The threshold model suggests both later onset of seismicity and lower seismicity rate prior to the increased network sensitivity in 1993.

While a qualitative comparison by eye strongly suggests that the fit to the Threshold model is

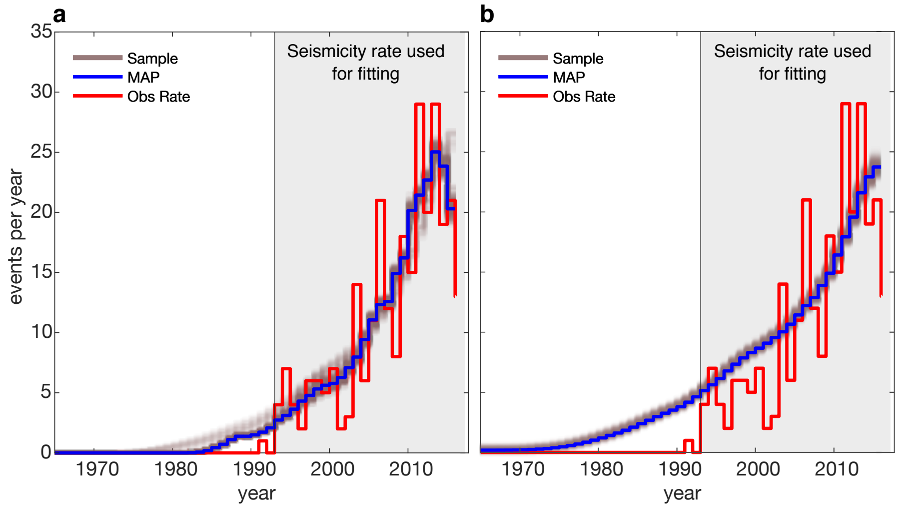


**Figure 2.** Time series fitting to seismicity rate where a is the threshold model and b is the Dieterich model. The seismicity rate before 1993 (outside gray box area) is not used in fitting. Red line is observed yearly rate filtered by the simplified completeness. Brown are plausible sampled models, blue line is the preferred model. Notice a much earlier onset of seismicity for the Dieterich model and that the model doesn't capture the decrease in the rate at the end of the time-series. We note that the drop in rate (red line) at the end of the time-series represents a further reduction in seismicity rate in the next year of 2017. However, this is beyond the time-scale of the stress model and not included in the modeled rate (e.g. blue).

significantly better than the original Dieterich (1994) (see Figure 2) it is worth testing quantitatively if the model fit is better given that the additional degree of freedom added by introduction of $\varDelta S_c$. Since the Dieterich (1994) model is fully nested in the new Threshold model (a limiting case where $\varDelta S_c = 0$), a simple F-test is appropriate for model comparison (Menke 2018). Using the MAP model (Figure 2), in both cases to compute the residual sum of squares the F-test indicates that the null hypothesis can be rejected with a $p = 0.015$. This therefore suggests that the improvement in fit is very likely significant.

The MCMC sampling provides constrains on model parameters. Based on 1 million samples for both models the following 95% confidence intervals are in Table 1. We stress, as was previously mentioned, that the confidence intervals are derived under the assumption of a small data variance and no additional sources of uncertainty and thus the parameter bounds may be smaller than for other approaches. Nevertheless the analysis reveals large uncertainty on some parameters and the intersection of confidence bounds for the two models implies strongly that they are in agreement.

First, we observe in Table 1 that the confidence bounds on the background rate $r$ of the two model, threshold and Dieterich (1994) intersects although the MAP values are quite different. However, the bounds on $A\sigma_0$ for the two models do not overlap, and the Threshold model is better fit with smaller

**Table 1.** List of MCMC sampling results rounded to two significant digits

| Model | Parameter | 95% conf. interval | MAP value | prior range | unit |
|---|---|---|---|---|---|
| Threshold | $r$ | $4.0 \cdot 10^{-6}$ – $3.2 \cdot 10^{-4}$ | $5.0 \cdot 10^{-6}$ | $6.3 \cdot 10^{-7}$ – $2.5 \cdot 10^{-3}$ | events/(year·km$^2$) |
| Dieterich | $r$ | $6.3 \cdot 10^{-5}$ – $1.3 \cdot 10^{-4}$ | $1.0 \cdot 10^{-4}$ | $6.3 \cdot 10^{-7}$ – $2.5 \cdot 10^{-3}$ | events/(year·km$^2$) |
| Threshold | $A\sigma_0$ | 0.0046 – 0.040 | 0.006 | 0.001 – 1 | MPa |
| Dieterich | $A\sigma_0$ | 0.041 – 0.050 | 0.045 | 0.001 – 1 | MPa |
| Threshold | $t_a$ | 720 – 9800 | 8700 | 0.5 – 10000 | years |
| Dieterich | $t_a$ | 9000 – 10000 | 10000 | 0.5 – 10000 | years |
| Threshold | $\Delta S_c$ | 0.07 – 0.18 | 0.17 | 0 – 0.5 | MPa |

value of $A\sigma_0$ than the Dieterich (1994) model. Most striking difference in the parameter estimates is seen in $t_a$. The threshold model doesn't place much constrain on $t_a$ since the confidence interval is nearly the prior range. However, the Dieterich (1994) model favors $t_a$ as large as possible and the samples cluster at the prior boundary at 10000 years. We tested expanding the prior further but found

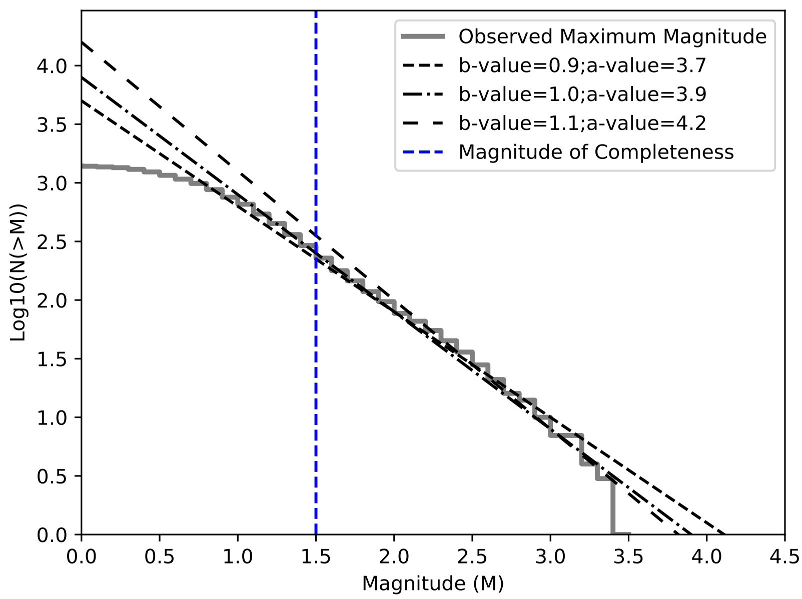


**Figure 3.** Magnitude-frequency distribution of earthquakes within the Groningen Gas field reported by KNMI (Koninkljjk Nederlands Meteorologisch Instituut, http://www.knmi.nl/) between 1991 and 2016 . N(>M) is number of earthquakes with magnitude larger than M. The vertical dashed blued line shows the estimated magnitude of completeness. We also show for reference the theoretical Gutenberg-Richter laws laws obtained for the most likely b-value (b=1.0) and the values bounding the 95% confidence range (b=0.88–1.12) determined by Bourne & Oates (2020).

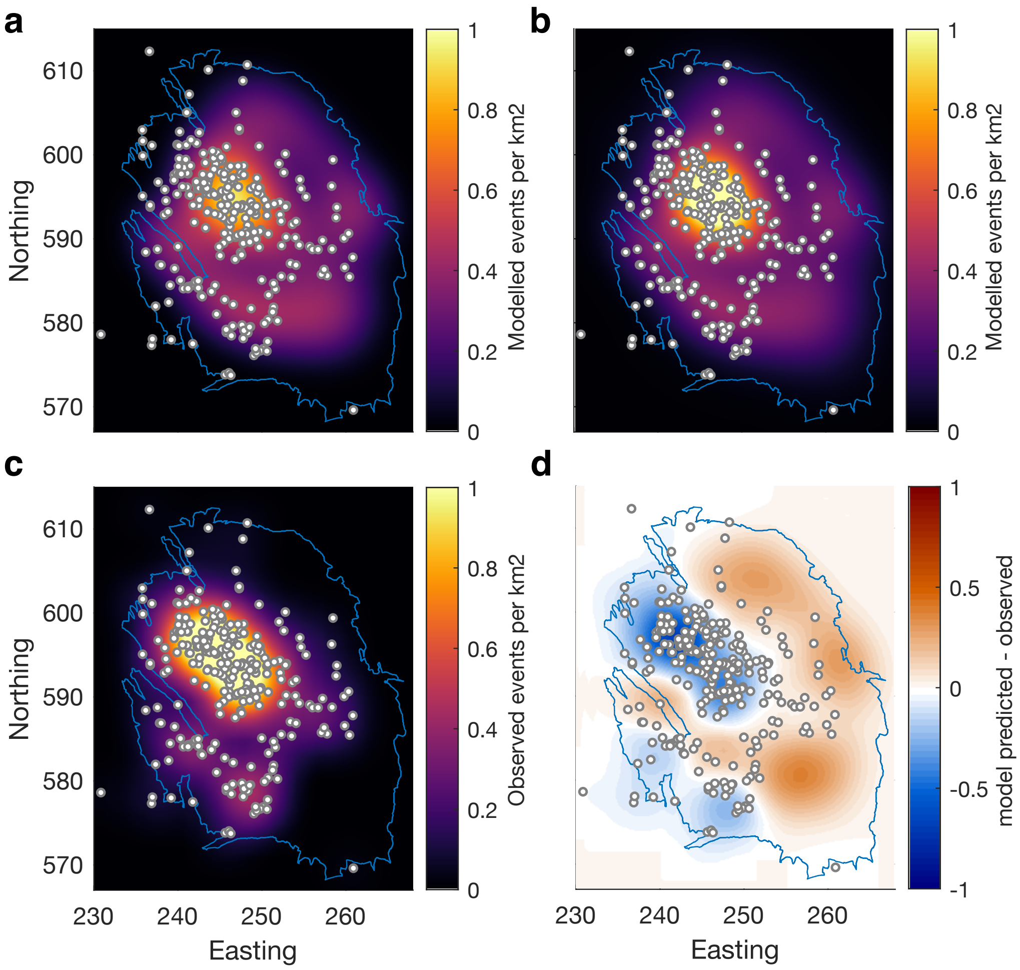


**Figure 4.** Spatial distribution of events in 2017. a: Model prediction of earthquake density by the threshold model with events plotted on top for references. b: Model prediction by the Dieterich model. c: Observed density with the same resolution as the model. d: Difference between observed density and threshold model density.

an only slightly improved fit. We discuss the implications of the $t_a$ estimate further in Section 4.1. Finally we obtained an value $\Delta S_c$ from the threshold model, but we highlight that if $\Delta S_c = 0$ then the Threshold model reduces to the Dieterich (1994) model. Thus another way to interpret the Dieterich values in Table 1 is that they represent the parameter estimate if $\Delta S_c$ is forced to be at the lower limit of the prior. Clearly the lower bound on acceptable $\Delta S_c$ is 0.07 MPa, which forces systematic differences in the two models and improves the fit for the Threshold model.

All spatial constrains for the seismicity rate come from the Coulomb stress field $\Delta S(t, x, y)$ reported by (Smith et al. 2021) and equation 4 doesn't explicitly penalize models depending on local spatial agreement such as Poissonian log-likelihood would. Nevertheless comparing the Threshold model (Figure 4a) and Dieterich (1994) model (Figure 4b) and the observed rate (Figure 4c) when

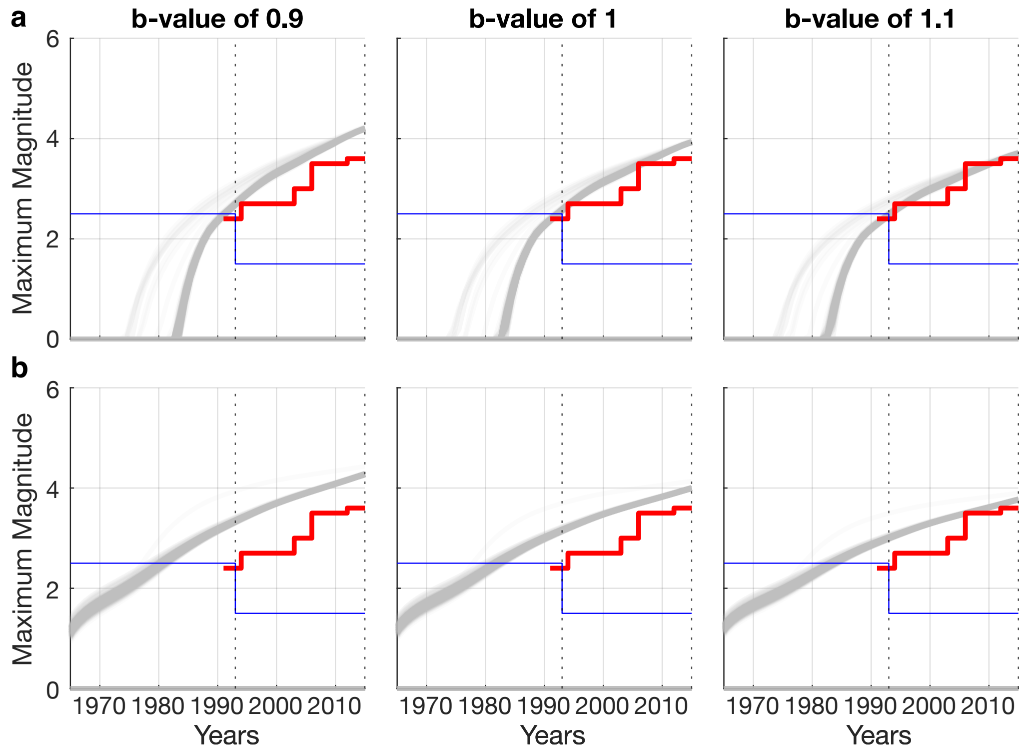


**Figure 5.** Analysis of model predicted maximum magnitude with time given a Gutenberg-Richter distribution. Gray lines are sampled probable models realizations given a b-value on top of each column. Red is the observed maximum magnitude. Blue is the simplified completeness magnitude. a (top row) uses the Threshold model. Notice that gray lines exceed completeness threshold about the same time as observed seismicity b (bottom row) uses the Dieterich model. Notice that the gray lines are well above the completeness threshold before any detected seismicity occurs.

the earthquake spatial distribution is filtered to the same length-scale of 3 km, which is the minimum resolvable length scale in the Coulomb stress formulations. We find both the Threshold model and Dieterich (1994) model to be in a reasonable agreement with the spatial distribution where in both cases the correlation of earthquake density in each block compared to the observed slightly exceeds 0.75. However, clear deficiencies are observed, in particular in the southeast of the gas field where the models over predict the seismicity rate.

To better assess if the Threshold model or the Dieterich (1994) model are in better agreement with the lack of observed seismicity prior to 1993, we compute the expected maximum magnitude (Van der Elst et al. 2016):

$$M_{max} = M_c + \frac{1}{b}\log_{10}(N), \tag{5}$$

where $b$ is the b-value of the Gutenberg-Richter distribution, which we have plotted and estimated for the catalog in Figure 3. $M_c$ is the magnitude of completeness, $N$ is the total cumulative number of events as predicted by integrating equation 1 or 2. Comparison of the two models to the observed maximum magnitude with time and the simplified completeness magnitude reveals (Figure 5) that for typical b-values the Threshold model is consistent with the lack of observed prior seismicity shows good agreement with the observed maximum magnitude for b-value 1 and 1.1. As seen in Figure 3, these values are in good agreement with the catalog used. However, the Dieterich (1994) model (Figure 5b) would suggest that magnitudes large enough to be detected should have occurred much earlier, furthermore, the agreement with observed maximum magnitude is poor for the explored b-values in Figure 5.

An independent determination of the b-value when the whole catalog is used was found to be around $1 \pm 0.12$ assuming no stress dependence of the b-value (Bourne & Oates 2020). We emphasize that the analysis in this section is based on the assumption that the $b$ value is constant in time and space, but some evidence suggests that this may not be the case (Bourne et al. 2014; Bourne & Oates 2020).

# 4 DISCUSSION

## 4.1 Parameter estimates

The most striking disparity in parameters estimates between the Threshold model and the Dieterich (1994) models is in the characteristic decay time $t_a$. The Dieterich (1994) model estimates this parameter to be very large and, in fact, the estimate is limited by the prior upper range at 10000 years (see Table 1). The Threshold model, on the other hand, does not place much constrain on the parameter.

The estimate of $t_a$ is critical to forecast the seismicity in response to any change of the production rate, in particular, once production ends. $t_a$ represents the time it takes the system to return to background seismicity rate following a stress step. Thus a large $t_a$ means a sustained seismic hazard for a long time. A short $t_a$ represents a rapid decline of seismic hazard. However, it is worth noting that in presence of deformation processes that would relax the imparted stresses then $t_a$ would over-estimate the duration of sustained seismic hazard level.

To investigate further the differences in the two models following a shut-in of production, we consider a scenario where in 2017 all production seized. We assume after shut-in the perturbations in the stress field are spatially and temporally constant. This is not rigorously the prediction for a shut-in in 2017 as the non-uniform pressure in the reservoir at the time of shut-in would imply be some small stress variations after shut in. It is, however, probably a close approximation that doesn't require

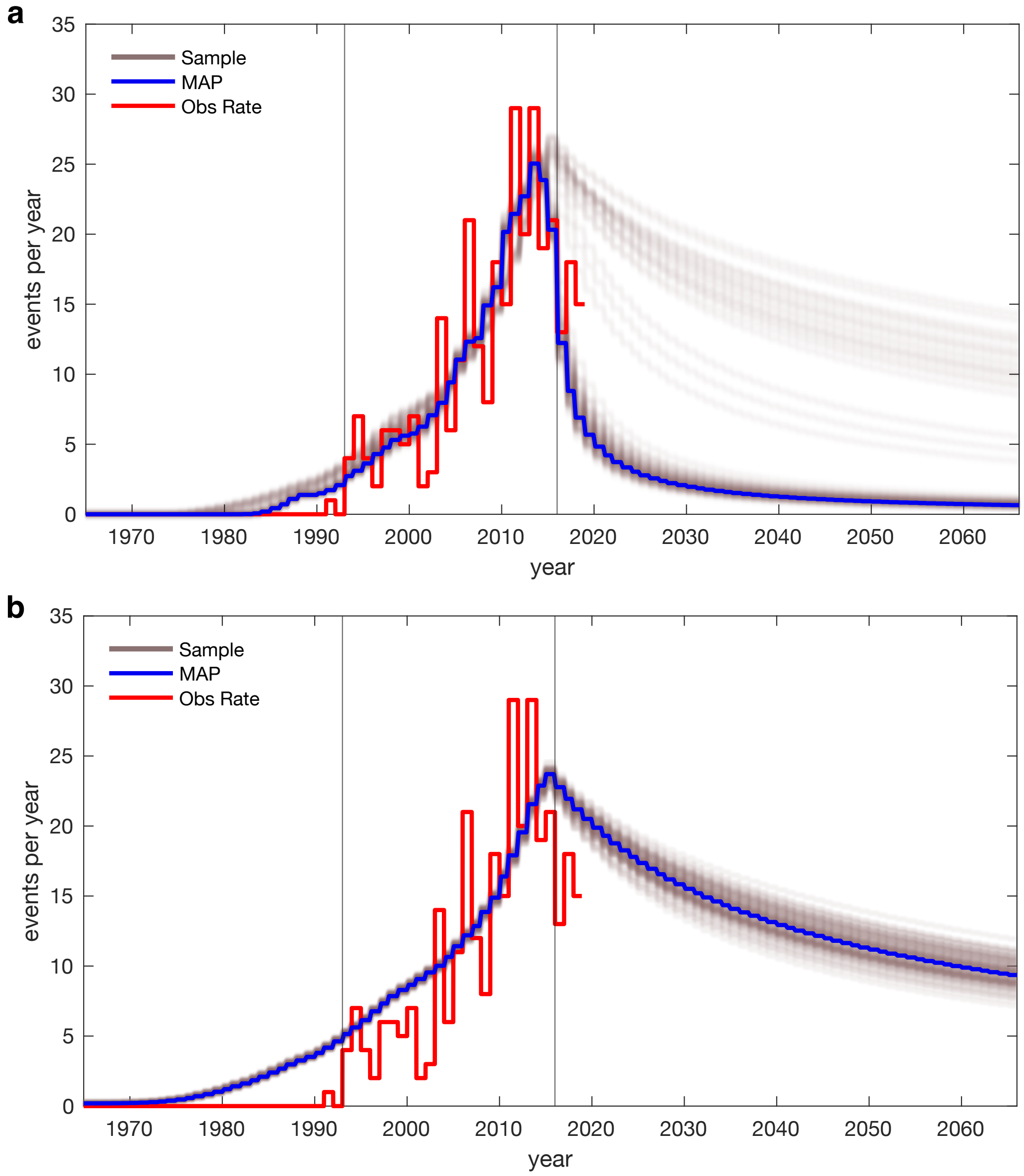


**Figure 6.** Seismicity rate for the Threshold model (a) and Dieterich (1994)'s model (b) after an abrupt hypothetical stop in production (shut-in) in 2017. The two vertical lines indicate the time-period used for model fitting and sampling. The Threshold model shows considerable variability following a shut-in, but most models show a fairly rapid decay of the seismicity rate, including the favored MAP model. However, all samples for the Dieterich (1994) model indicate a fairly slow decay of the seismicity rate and suggest a substantially elevated seismic risks for several decades after shut-in

reservoir modeling and is sufficient to illustrate how the forecast differs if a threshold is introduced in the Dieterich (1994) model.

Figure 6 demonstrates clearly the differences in the two models. The Threshold model shows some variability in how the seismicity rate decays, however, most realizations cluster around the MAP model that indicates rapid decay of the seismicity rate in the decades following shut-in. The variability is most likely explained by the fact that $t_a$ is not well constrained by the optimization period, but the hypothetical scenario presented indicates that a shut-in procedure would place considerable constrains on the $t_a$ parameter in the next few years after shut-in.

Much less variability is observed after shut-in from Dieterich (1994)'s model (Figure 6b), furthermore, all realizations suggest a substantially elevated seismicity for several decades after the shut-in. Thus applying the Dieterich (1994) model to the Groningen dataset implies that increased seismicity rate may be observed for very long time following a stop in production at Groningen, however, the threshold model suggests that $t_a$ can't be well determined with the available data, but could be much smaller than suggested by the application of the model of Dieterich (1994). In summary, it is evident that if these model are used to perform a seismic hazard analysis for various end-of-production scenarios they would render significantly different results.

Another critical difference of the parameter estimates manifests in that the Dieterich (1994) model represents a limiting case of the Threshold model where the threshold $\Delta S_c = 0$. It is worth highlighting that all parameters are assumed spatially constant, including $\Delta S_c$ but the stress field $\Delta S(t', x, y)$ is not (Smith et al. 2021). Thus the threshold is reached at different times in different places. Firstly, this distinguishes the model from the critical time model of Zhai et al. (2019) where the critical time represented a regional activation of seismicity regardless of local stress state. Secondly, estimating $\Delta S_c$ may have predictive value for activation of seismicity in areas of small stress as production or injection continues.

### 4.2 Unmodeled variance

For further analyzing the discrepancy in model and data we compute a $\chi^2_\nu$ value, that is chi-squared reduced value, (e.g. Menke 2018)

$$\chi^2_\nu = \frac{1}{\nu} \sum_{i=1993}^{i=2016} \left( R^o_y - \int_\Sigma R(\boldsymbol{m}, i, x, y) dx dy \right)^2, \tag{6}$$

where $\nu$ is the degrees of freedom ($\nu$ =19 for the Threshold model, $\nu$ =20 for the Dieterich (1994) model) and we have taken the variance as 1 (see Appendix C for explanation). $\chi^2_\nu$ value significantly larger than 1 indicates a poor fit, or an underestimation of the variance. $\chi^2_\nu$ value significantly less than 1 indicates usually over fitting. Thus a $\chi^2_\nu \approx 1$ is indicative of a fit that is in agreement with the variance.

Using the MAP model (Figure 2) and the observed rate we obtain $\chi^2_\nu = 19.3$ for the Threshold

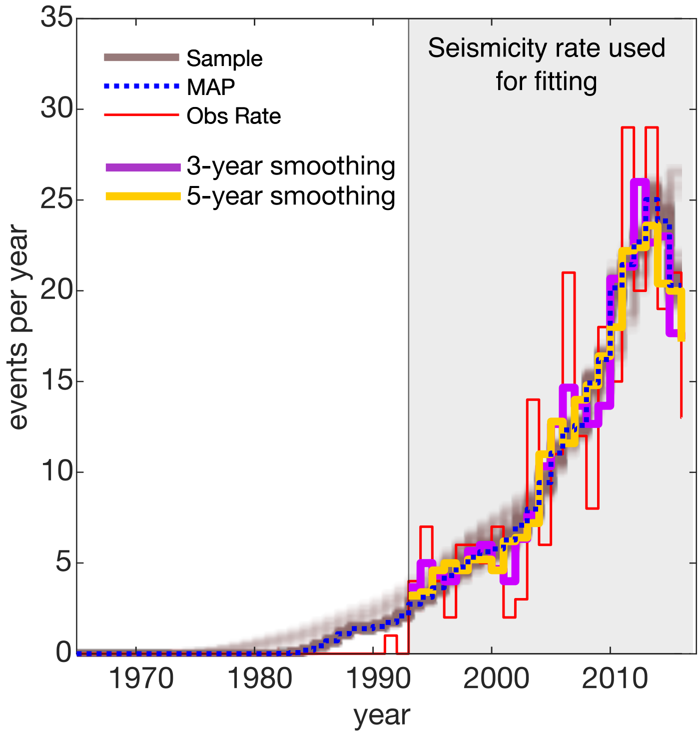


**Figure 7.** A modification of Figure 2a where we have added 3 and 5 year running average smoothing of the observed rate. This reveals a remarkably good agreement between the MAP model (dashed blue), which represents that optimal model constrained on the data in red given the priors, and the 5 year smooth (yellow)

model and $\chi^2_\nu = 25.3$ for the Dieterich (1994) model. Although the Threshold model performs better, the large value of $\chi^2_\nu$ indicates that the variance is severely underestimated.

However, we observe that model appears to average the various fluctuations in the observed rate with time. Thus we test computing $\chi^2_\nu$ after 3 and 5 year running mean smoothing (Figure 7) using the same model as before (constrained by the red line data). We obtain $\chi^2_\nu = 2.77$ and 1.36 for 3 and 5 year smoothing respectively (Figure 7, purple and yellow) for the Threshold model. We find $\chi^2_\nu = 8.94$ and 6.07 for 3 and 5 year smoothing respectively for the Dieterich (1994) model (not plotted). This implies a close to ideal $\chi^2_\nu$ value for 5-year smoothing if the Threshold model is used and some improvement for the Dieterich (1994) model although still significantly larger than 1.

We suggest two interpretations of this result that need further investigation. Firstly, the averaging by a running mean may be compensating for temporal custering occuring on a long time scale of about 3–5 years. This would be in agreement with the interacting rate-and-state model of Heimisson (2019) where interactions where not found to change the average number of events on long time-scales. This finding may also be in agreement with recent results of Post et al. (2021) that suggested that about 27% of the Groningen catalog may be triggered events. Secondly, the variance model used in this study is reasonably justified, from an obeservational point of view, if the goal is not to model short term variations in the seismicity rate.

### 4.3 Poissonian log-likelihood

It is a more common practice to carry out optimization and model comparison of seismicity rate models using a Poissonian log-likelihood (e.g. Ogata 1998) model rather than a Gaussian log-likelihood as has been done here. It is thus worth discussion the rational for out choice.

The choice of a Poissonian log-likelihood is a motivated by two main reasons. Firstly, that earthquake rates are count rates and thus negative values are non-physical. Second, that studies have shown that earthquakes are Poissonian point processes (e.g. Gardner & Knopoff 1974). However, the latter property is contingent on removing temporal clustering, or aftershocks, which cause temporal correlation in the rate and violate the Markov property of a Poissonian process. The declustering process is nonunique where different algorithms, intended for the same purpose, can render different results (e.g. Marsan & Lengline 2008; Mizrahi et al. 2021). Declustering is particularly problematic for induced seismicity where the external forcing imposes spatial and temporal correlation of events superimposed on aftershock correlation. Declustering in these cases has been found to lead to counter-intuitive decision making and results (Maurer et al. 2020).

However, the principal reason we do not use a Poissonian log-likelihood function in this study is that the threshold model will take a value of $R = 0$ before the threshold is reached. This means that Poissonian log-likelihood function assigns exactly 0 probability to models where an event is observed but the theoretical rate is zero ($R = 0$). We tested using a Poissonian log-likelihood from Ogata (1998) for sampling, but found this property to lead to restrictive sampling and poor fit. Considering all the uncertainty in the stress modeling, event locations, and the theoretical seismicity rate model it seemed inappropriate to pick such a restrictive likelihood model that rejects a model if a single event is found in a region where the rate is zero. We considered resolutions such as removing data points if this violation occurs. However, that would change the degrees of freedom as a function of the model parameters and would render model comparison difficult to interpret.

### 4.4 Models with time-dependent or instantaneous stress triggering

The model we have presented assumes the earthquake nucleation process is time-dependent and described by a spring-slider and rate-and-state friction. However, Smith et al. (2021) explored seismicity rate forecasting models, which assume that nucleation is instantaneous, dependent on a failure stress distribution, and thus do not have an explicit time-dependence. Much like in this study Smith et al. (2021) observed an excellent agreement with the observed rate by using models that effectively incorporate an threshold stress. This comparison begs the question: Does the time-dependence of friction matter when modeling the Groningen induced seismicity?

A possible explanation may be provided in Table 1 where it is revealed that $t_a$ is not well determined by the data. By looking at equation 1 we notice that $1/t_a$ shows up multiplying the time-integral in the denominator. The fact that $t_a$ is not constrained implies that the integral is not important to constrain the fit. If this integral is ignored then the model reduces to the instantaneous limit of the equation, valid at early time shortly after $t_b$:

$$\begin{aligned} \frac{R}{r} &= \exp\left(\frac{\Delta S(t) - \Delta S_c}{A\sigma_0}\right) && \text{if } t \geq t_b \\ \frac{R}{r} &= 0 && \text{if } t < t_b, \end{aligned} \tag{7}$$

which is not explicitly time-dependent much like models explored by Smith et al. (2021) and furthermore takes on a similar functional form as the extreme threshold model (Bourne et al. 2018):

$$R_{ET} \propto \theta_1 \frac{d\Delta S}{dt} \exp\left(\theta_1 \Delta S(t) + \theta_0\right) \tag{8}$$

Where $R_{ET}$ is the extreme threshold distribution seismicity rate and $\theta_0$, $\theta_0$ are statistical parameter characterizing the shape of the distribution.

We suggest that discriminating between the time-dependent friction model presented here and the instantaneous triggering models Smith et al. (2021) can be achieved by investigating shorter time-intervals. Groningen has seasonal fluctuations in the production rate (Bourne et al. 2014). We expect that such short-term but large amplitude fluctuations will manifest differently in the model presented here compared to the Smith et al. (2021) models. From a physical point of view; an ongoing nucleation can be modulated by the stress fluctuation. From a mathematical point of view; significant differences are expected since in the Smith et al. (2021) models the seismicity rate scales with stressing rate as in equation 8, which can become negative and thus needs some type of regularization, such as imposing a non-negativity or a Kaiser effect, to avoid nonphysical effects. Such modifications necessarily introduce non-uniqueness dependent on the users' choice of regularization. However, in the Dieterich (1994) class of models there is no explicit dependence of seismicity rate on the time-derivative of stress. Thus the model maintains validity even for negative stressing rates or non-differentiable stressing histories. In conclusion, we suggests that for Groningen and by investigating yearly seismicity rate that we cannot discriminate between models that assume time-dependent friction and time-independent friction.

## 5 CONCLUSIONS

We have presented a new Coulomb rate-and-state model (equation 1) that assumes sources can initially be well below steady state. The derivation of the model (Appendix A and B) shows that a simple stress threshold $\varDelta S_c$ is needed, regardless of stressing history, to bring the seismic source above steady state. We have compared the new Threshold model to the original Dieterich (1994) model using the data from the Groningen gas field in the Netherlands. We obtain much improved agreement using the Threshold model in terms of time-series fitting to the observed seismicity rate and better agreement with the observed maximum magnitute with time. The two model provide similar agreement in terms of spatial distribution of events.

## ACKNOWLEDGMENTS

E.R.H. formulated the main research questions in consultation with J-P.A. and S.J.B. E.R.H. derived the threshold model, and carried out data and model comparison. E.R.H. and J.D.S. developed code and methods for data and model comparison and visualization. J-P.A. and S.J.B helped interpret results. E.R.H wrote the manuscript with input from all authors.

E.R.H. acknowledges support from the Geophysics Option Postdoctoral Fellowship at Caltech.J.S. was supported for this project by the NSF centre of Geomechanics and Mitigation of Geohazards (GMG). We gratefully acknowledge data and support from Nederlandse Aardoli Maatschappij (Jan Van Elk, Gini Ketellar and Dirk Doornhof), Shell Global Solutions (Stijn Bierman, Steve Oates, Rick Wentinck, Xander Campman, Alexander Droujinine and Chris Harris), and Koninkljjk Nederlands Meteorologisch Instituut for the open source earthquake location information. (http://www.knmi.nl/). We thank the IUCRC program of the National Science Foundation for support though grant 1822214 to GMG.

## DATA AVAILABILITY

Data used in this paper, from which the stress model is derived, has been previously published in Smith et al. (2019). Seismic data and catalogs are provided by Koninkljjk Nederlands Meteorologisch Instituut (http://www.knmi.nl/).

## REFERENCES

Bourne, S. J. & Oates, S. J., 2017. Extreme threshold failures within a heterogeneous elastic thin sheet and the spatial-temporal development of induced seismicity within the groningen gas field, *Journal of Geophysical*

*Research: Solid Earth*, **122**(12), 10,299–10,320.

Bourne, S. J. & Oates, S. J., 2020. Stress-dependent magnitudes of induced earthquakes in the groningen gas field, *Journal of Geophysical Research: Solid Earth*, **125**(11), e2020JB020013.

Bourne, S. J., Oates, S. J., van Elk, J., & Doornhof, D., 2014. A seismological model for earthquakes induced by fluid extraction from a subsurface reservoir, *Journal of Geophysical Research: Solid Earth*, **119**(12), 8991–9015.

Bourne, S. J., Oates, S. J., & van Elk, J., 2018. The exponential rise of induced seismicity with increasing stress levels in the Groningen gas field and its implications for controlling seismic risk, *Geophysical Journal International*, **213**(3), 1693–1700.

Candela, T., Osinga, S., Ampuero, J.-P., Wassing, B., Pluymaekers, M., Fokker, P. A., van Wees, J.-D., de Waal, H. A., & Muntendam-Bos, A. G., 2019. Depletion-induced seismicity at the groningen gas field: Coulomb rate-and-state models including differential compaction effect, *Journal of Geophysical Research: Solid Earth*, **124**(7), 7081–7104.

Cattania, C., Hainzl, S., Wang, L., Roth, F., & Enescu, B., 2014. Propagation of coulomb stress uncertainties in physics-based aftershock models, *Journal of Geophysical Research: Solid Earth*, **119**(10), 7846–7864.

Dieterich, J., 1994. A constitutive law for rate of earthquake production and its application to earthquake clustering, *Journal of Geophysical Research: Solid Earth*, **99**(B2), 2601–2618.

Dieterich, J. H., 1979. Modeling of rock friction: 1. experimental results and constitutive equations, *Journal of Geophysical Research: Solid Earth*, **84**(B5), 2161–2168.

Dost, B., Ruigrok, E., & Spetzler, J., 2017. Development of seismicity and probabilistic hazard assessment for the groningen gas field, *Netherlands Journal of Geosciences*, **96**(5), s235–s245.

Ellsworth, W. L., 2013. Injection-induced earthquakes, *Science*, **341**(6142).

Foreman-Mackey, D., Hogg, D. W., Lang, D., & Goodman, J., 2013. emcee: the mcmc hammer, *Publications of the Astronomical Society of the Pacific*, **125**(925), 306.

Gardner, J. & Knopoff, L., 1974. Is the sequence of earthquakes in southern california, with aftershocks removed, poissonian?, *Bulletin of the Seismological Society of America*, **64**(5), 1363–1367.

Goodman, J. & Weare, J., 2010. Ensemble samplers with affine invariance, *Communications in applied mathematics and computational science*, **5**(1), 65–80.

Hainzl, S., Steacy, D., & Marsan, S., 2010. Seismicity models based on Coulomb stress calculations, *Community Online Resource for Statistical Seismicity Analysis*, Available at http://www.corssa.org.

Heimisson, E. R., 2019. Constitutive law for earthquake production based on rate-and-state friction: Theory and application of interacting sources, *Journal of Geophysical Research: Solid Earth*, **124**(2), 1802–1821.

Heimisson, E. R. & Segall, P., 2018. Constitutive law for earthquake production based on rate-and-state friction: Dieterich 1994 revisited, *Journal of Geophysical Research: Solid Earth*, **123**(5), 4141–4156.

Hogg, R. V., McKean, J., & Craig, A. T., 2019. *Introduction to mathematical statistics, Eigth Edition*, Pearson Education.

Linker, M. F. & Dieterich, J. H., 1992. Effects of variable normal stress on rock friction: Observations and constitutive equations, *J. Geophys. Res. Solid Earth*, **97**(B4), 4923–4940.

Marone, C., 1998. Laboratory-derived friction laws and their application to seismic faulting, *Annu. Rev. Earth Pl. Sc.*, **26**(1), 643–696.

Marsan, D. & Lengline, O., 2008. Extending earthquakes' reach through cascading, *Science*, **319**(5866), 1076–1079.

Maurer, J., Kane, D., Nyst, M., & Velasquez, J., 2020. Risk from oklahoma's induced earthquakes: The cost of declustering, *Bulletin of the Seismological Society of America*.

Menke, W., 2018. *Geophysical data analysis: Discrete inverse theory*, Academic press.

Mizrahi, L., Nandan, S., & Wiemer, S., 2021. The Effect of Declustering on the Size Distribution of Mainshocks, *Seismological Research Letters*.

Nederlandse Aardolie Maatschappij, 2013. A technical addendum to the winningsplan groningen 2013 subsidence, induced earthquakes and seismic hazard analysis in the groningen field, *NAM, Assen*.

Norbeck, J. H. & Rubinstein, J. L., 2018. Hydromechanical earthquake nucleation model forecasts onset, peak, and falling rates of induced seismicity in oklahoma and kansas, *Geophysical Research Letters*, **45**(7), 2963–2975.

Ogata, Y., 1998. Space-time point-process models for earthquake occurrences, *Annals of the Institute of Statistical Mathematics*, **50**(2), 379–402.

Post, R. A., Michels, M. A., Ampuero, J.-P., Candela, T., Fokker, P. A., van Wees, J.-D., van der Hofstad, R. W., & van den Heuvel, E. R., 2021. Interevent-time distribution and aftershock frequency in non-stationary induced seismicity, *Scientific reports*, **11**(1), 1–10.

Richter, G., Hainzl, S., Dahm, T., & Zöller, G., 2020. Stress-based, statistical modeling of the induced seismicity at the groningen gas field, the netherlands, *Environmental Earth Sciences*, **79**, 1–15.

Ruina, A., 1983. Slip instability and state variable friction laws, *Journal of Geophysical Research: Solid Earth*, **88**(B12), 10359–10370.

Smith, J. D., Avouac, J.-P., White, R. S., Copley, A., Gualandi, A., & Bourne, S., 2019. Reconciling the long-term relationship between reservoir pore pressure depletion and compaction in the groningen region, *Journal of Geophysical Research: Solid Earth*, **124**(6), 6165–6178.

Smith, J. D., White, R. S., Avouac, J.-P., & Bourne, S., 2020. Probabilistic earthquake locations of induced seismicity in the groningen region, the netherlands, *Geophysical Journal International*, **222**(1), 507–516.

Smith, J. D., Heimisson, E. R., Bourne, S. J., & Avouac, J.-P., 2021. Stress-based forecasting of induced seismicity with instantaneous earthquake failure functions: Applications to the groningen gas reservoir., *???*, **???**

Van der Elst, N. J., Page, M. T., Weiser, D. A., Goebel, T. H., & Hosseini, S. M., 2016. Induced earthquake magnitudes are as large as (statistically) expected, *Journal of Geophysical Research: Solid Earth*, **121**(6), 4575–4590.

Willacy, C., van Dedem, E., Minisini, S., Li, J., Blokland, J.-W., Das, I., & Droujinine, A., 2019. Full-waveform event location and moment tensor inversion for induced seismicity, *Geophysics*, **84**(2), KS39–KS57.

Zhai, G., Shirzaei, M., Manga, M., & Chen, X., 2019. Pore-pressure diffusion, enhanced by poroelastic stresses, controls induced seismicity in oklahoma, *Proceedings of the National Academy of Sciences*, **116**(33), 16228–16233.

## APPENDIX A: TIME TO ACTIVATION: SINGLE SOURCE

We start by describing a single seismic source, idealized as a spring and slider system, which is at time $t = 0$ well below steady state. We shall refer to seismic source well below steady state as inactive. Here we shall see that if all seismic sources in a population are inactive there will be no seismicity produced until we reach a certain stress where they become active. We investigate the state evaluation equation (Dieterich 1979; Ruina 1983),

$$\dot{\theta} = 1 - \frac{\dot{\delta}\theta}{d_c} = 1 - \mathit{\Omega} \tag{A.1}$$

If $\mathit{\Omega} \gg 1$, the source is accelerating towards instability (active and well above steady state), if $\mathit{\Omega} \ll 1$ the source is in healing phase (inactive and well below steady state). If $\mathit{\Omega} = 1$ the source is at steady state ($\dot{\theta} = 0$).

Assuming $\mathit{\Omega} \ll 1$, then

$$\theta = \theta_0 + t. \tag{A.2}$$

The rate-and-state friction law and force balance becomes (following notations of Heimisson & Segall (2018))

$$\tau(t) - k\delta(t) = \sigma(t)\left(\mu + A\log\frac{\dot{\delta}(t)}{V^*} + B\log\frac{(\theta_0 + t)V^*}{d_c}\right) \tag{A.3}$$

Rearranging provides:

$$K(t)\left(\frac{\theta_0}{\theta_0 + t}\right)^{(B/A)} = \frac{\dot{\delta}}{\dot{\delta}_0}\exp\left(\frac{-k\delta}{A\sigma(t)}\right) \tag{A.4}$$

Where

$$K(t) = \exp\left(\frac{\tau(t)}{A\sigma(t)} - \frac{\tau_0}{A\sigma_0}\right) \approx \exp\left(\frac{\mathit{\Delta} S(t)}{A\sigma_0}\right) \tag{A.5}$$

where the approximation is the Coulomb stress approximation discussed in detail by Heimisson & Segall (2018). In other words, $\mathit{\Delta} S(t) = \tau(t) - \mu\sigma(t)$ represents modified Coulomb stress, with $\mu = \tau_0/\sigma_0 - \alpha$. $\tau_0$ and $\sigma_0$ are the initial background shear and effective normal stress respectively, $\alpha$ is the Linker-Dieterich constant (Linker & Dieterich 1992).

If a seismic source is well below steady state it will slip a very small distance until it will be perturbed sufficiently to go above steady state. We thus assume in Eq. A.4 that $k\delta/A\sigma_0 \ll 1$ and thus:

$$\frac{\dot{\delta}}{\dot{\delta}_0} = K(t)\left(\frac{\theta_0}{\theta_0 + t}\right)^{(B/A)} \tag{A.6}$$

If the seismic sources have been healing for much longer time than they are perturbed then $\theta_0 \gg t$. This is likely always true for seismically inactive faults that have been healing for geological time-scales, but are perturbed on the time scale of months to years. Thus:

$$\frac{\dot{\delta}}{\dot{\delta}_0} = K(t) \tag{A.7}$$

Now let us assume that a source actives at $\Omega_c \gtrsim 1$, but $\Omega_c = 1$ is exactly steady-state. Then we find a critical stress perturbation $\Delta S_c$ (using the Coulomb stress approximation).

$$\frac{\Delta S_c}{A\sigma_0} = \log\left(\frac{\Omega_c}{\Omega_0}\right) \tag{A.8}$$

By virtue of the slow growth of the logarithm we may infer from equation A.8 that perturbations of the order of $A\sigma_0$ are universally needed to activate the population. Once the threshold is achieved the assumption of well above steady state is justified and the Dieterich theory can be applied. Then the time $t_b$ at which the seismic source is activated is the solution of the following equation:

$$\Delta S(t = t_b) = \Delta S_c = A\sigma_0 \log\left(\frac{\Omega_c}{\Omega_0}\right), \tag{A.9}$$

where we infer that the critical stress $\Delta S_c$ will typically be in the range of 1 – 10 $A\sigma_0$. In practical applications either $\Delta S_c$ or $t_b$ needs to be determined. This estimations may be done through an inversion process, but it is worth noting that typically $t_b$ can considered an observable, at least up to reasonable certainty. It would then represent the time since injection, extraction, or other perturbations started until the time that seismic activity begins. However, If the stress perturbation in space is heterogeneous then $t_b$ will also likely vary in space. Through a stress model and an estimation of $A\sigma_0$ one can relate $t_b$ to $\Delta S_c$, which may not vary strongly in space due to logarithmic dependence on $\Omega_c/\Omega_0$ and could potentially have a predictive value for the onset of seismicity in other regions. It may, therefore, be more straightforward to directly invert for $\Delta S_c$, assuming that it is spatially uniform, instead of estimating $t_b$.

## APPENDIX B: NEW CONSTITUTIVE LAW: A THRESHOLD MODEL

In the previous section we derived a stress threshold $\Delta S_c$ at which a seismic source can be considered active or above steady state. Now we assume that once we reach $\Delta S_c$ the whole population of seismic sources is moved above steady state, in other word, all sources become active. This assumptions is likely reasonable as long as the variability of $\Delta S_c$ in the populations of seismic sources is less than $A\sigma_0$. Further, for the sake of mathematical tractability, we assume the sources cannot be moved below steady state once it is well above steady state or activated.

By assuming that the seismic sources under arbitrary stressing conditions are activated at time $t = t_b$ and for background conditions at $t_b^o$ then equation 17 in Heimisson & Segall (2018) can be rewritten in the following manner:

$$\int_{t_b}^{t} K(t')dt' = \int_{t_b^o}^{t_b^o+N/r} e^{t'/t_a} dt', \tag{B.1}$$

where $t_b$ is a constant and represents the time when $\Delta S(t = t_b) = A\sigma_0 \log(\frac{\Omega_c}{\Omega_0})$, $t_b^o = t_a \log(\frac{\Omega_c}{\Omega_0}) = t_a \Delta S_c/(A\sigma_0)$. Thus implementing the Coulomb stress approximation, which will be used to replace $K(t)$ hereafter, we find:

$$\int_{t_b}^{t} \exp\left(\frac{\Delta S(t')}{A\sigma_0}\right) dt' = t_a \frac{\Omega_c}{\Omega_0}\left(e^{N/rt_a} - 1\right). \tag{B.2}$$

Solving for $N$ gives

$$\frac{N}{r} = t_a \log\left(\frac{1}{t_a \frac{\Omega_c}{\Omega_0}} \int_{t_b}^{t} \exp\left(\frac{\Delta S(t)}{A\sigma_0}\right) dt' + 1\right), \tag{B.3}$$

or alternatively

$$\frac{N}{r} = t_a \log\left(\frac{1}{t_a} \int_{t_b}^{t} \exp\left(\frac{\Delta S(t) - \Delta S_c}{A\sigma_0}\right) dt' + 1\right), \tag{B.4}$$

Comparison to equation 18 in Heimisson & Segall (2018) and equation B.4 B.4 reveals that the theory proposed here reduced to the Dieterich (1994) theory in the limit when the threshold stress $\Delta S_c = 0$, as should be expected. Were we note that $N = 0$ it $t < t_b$. Seismicity rate $R$ is found by differentiation:

$$\frac{R}{r} = \frac{K(t)}{\left(\frac{1}{t_a}\int_{t_b}^{t} K(t')dt' + \frac{\Omega_c}{\Omega_0}\right)} \tag{B.5}$$

or alternatively

$$\frac{R}{r} = \frac{\exp\left(\frac{\Delta S(t)-\Delta S_c}{A\sigma_0}\right)}{\frac{1}{t_a}\int_{t_b}^{t}\exp\left(\frac{\Delta S(t')-\Delta S_c}{A\sigma_0}\right)dt' + 1}, \tag{B.6}$$

which is equation 1 in the maintext.

## APPENDIX C: DERIVATION OF SEISMICITY-RATE VARIANCE

Here we derive the simple variance model that is used in the study to characterize the uncertainty in the binned seismicity rate.

First we note the Poissonian probability distribution

$$P(X = x_i) = \frac{e^{-\lambda}\lambda^{x_i}}{x_i!}, \tag{C.1}$$

where $\lambda$ is the expected value of $X$, which we interpret in this study as the number of events in some time-interval, and also the variance of $X$.

The distribution of $n$ samples from the distribution is also a Poisson distribution of random variable $Y = \sum_{i=1}^{n} x_i$ with the expected value of $n\lambda$ (e.g. Hogg et al. 2019, theorem 3.2.1) thus

$$P(Y = \sum_{i=1}^{n} x_i) = \frac{e^{-n\lambda}(n\lambda)^{\sum_{i=1}^{n} x_i}}{(\sum_{i=1}^{n} x_i)!}. \tag{C.2}$$

where $\sum_{i=1}^{n} x_i = 0, 1, 2, \ldots$. The distribution of the sample mean $\bar{X}$ can be obtained by substitution $\sum_{i=1}^{n} x_i = n\bar{X}$

$$P(\bar{X} = \bar{x}) = \frac{e^{-n\lambda}(n\lambda)^{n\bar{x}}}{(n\bar{x})!}, \tag{C.3}$$

where $\bar{x} \in \{0, 1/n, 2/n, \ldots\}$ or alternatively $\bar{x} = j/n$, where $j \in \{0, 1, 2, \ldots\}$. We can thus compute the expected value of the sample mean distribution:

$$\langle \bar{X} \rangle = \sum_{j=0}^{\infty} \frac{j}{n} \frac{e^{-n\lambda}(n\lambda)^j}{j!} = \lambda. \tag{C.4}$$

This is not unexpected since we the mean of the sample mean distribution must also be the mean of the distribution that is being sampled. However, the same is not true for the variance.

$$\mathrm{Var}(\bar{X}) = \sum_{j=0}^{\infty} \left(\frac{j}{n} - \lambda\right)^2 \frac{e^{-n\lambda}(n\lambda)^j}{j!} = \frac{\lambda}{n}. \tag{C.5}$$

Thus the variance of the sample mean is reduced the more samples are used, as is expected.

In our case we estimate the characteristic rate $R$ as the number of events $n$ divided by the bin length. Then $\lambda = R\Delta t$, but the time interval $\Delta t$ is also the bin length, thus the estimate of the variance is simply 1.